Multiiron Polyoxoanions. Synthesis, Characterization, X-ray Crystal Structure, and Catalytic H_2O_2-Based Alkene Oxidation by [(*n*-C_4H_9)$_4$N]$_6$[Fe$^{III}_4$(H_2O)$_2$(PW$_9$O$_{34}$)$_2$][†]

Xuan Zhang, Qin Chen, Dean C. Duncan, Rene J. Lachicotte,[‡] and Craig L. Hill*

Department of Chemistry, Emory University, Atlanta, Georgia 30322

Received April 4, 1997[⊗]

A tetranuclear ferric Keggin sandwich-type heteropolyanion has been synthesized by the reaction of the lacunary species Δ-Na$_8$H[PW$_9$O$_{34}$] with FeCl$_2$ followed by O$_2$ oxidation in nonaqueous media. The structure of [(*n*-C$_4$H$_9$)$_4$N]$_6$[Fe$^{III}_4$(H$_2$O)$_2$(PW$_9$O$_{34}$)$_2$]·4CH$_3$CN·2CH$_2$Cl$_2$·2H$_2$O (TBA-**1**) was determined by single-crystal X-ray diffraction (orthorhombic, *Pbca*; R = 0.0693 for 14 963 reflections with F_o > 4σ(F_o)). The compound was further characterized by infrared and UV−visible spectroscopy, electrochemistry, magnetic susceptibility, FAB mass spectrometry (FAB-MS), and elemental analyses. Five lines of evidence are consistent with the Fe$^{III}_4$ oxidation state: (i) valence sum calculations from the X-ray structure (ca. 2.86 ± 0.07 per Fe); (ii) the rest potential from cyclic voltammetry; (iii) charge balance requirements; (iv) titration with Ce^{IV}(SO$_4$)$_2$; and (v) oxidation by O$_2$. In contrast to the tetranuclear ferric Wells−Dawson-derived sandwich complex, [Fe$^{III}_4$(H$_2$O)$_2$(P$_2$W$_{15}$O$_{56}$)$_2$]$^{12-}$, TBA-**1** can only be prepared from a ferrous precursor. TBA-**1** is a catalyst for the oxidation of hydrocarbons with H$_2$O$_2$. The selectivity for epoxide is low (10−50%). Unlike most other transition-metal-substituted polyoxometalates (TMSPs), TBA-**1** is very stable under turnover conditions in aqueous H$_2$O$_2$ (no detectable changes in the IR or NMR spectra after 48 h). The rate of H$_2$O$_2$ disproportionation catalyzed by TBA-**1** is relatively low (the ratio of rates, disproportionation to oxidation, is ca. 3:2).

Introduction

The oxidation of hydrocarbons by the environmentally and economically attractive oxidants H$_2$O$_2$ and O$_2$ catalyzed by homogeneous metal complexes in Nature and in industry alike continues to be a focus of considerable current research.[1−6] The recent availability of X-ray crystal structures combined with significant spectroscopic information on methane momooxygenase (MMO)[7] and ribonucleotide diphosphate reductase (RDPR)[2,8] has defined a defensible platform from which to investigate the modes of action of the Fe$_2$ active sites of these enzymes. Paralleling this effort, synthetic complexes designed to model the non-heme Fe enzyme active sites have continued to develop rapidly.[5,6] Complementing these bioinorganic ventures is the development of homogeneous completely inorganic oxidatively resistant multimetal-based complexes that catalyze organic oxidations by H$_2$O$_2$ with rates, selectivities, and stabilities that define some pragmatic potential.[9−13]

The polyoxoanion of focus, [Fe$^{III}_4$(H$_2$O)$_2$(PW$_9$O$_{34}$)$_2$]$^{6-}$, **1** (Figure 1), is structurally related to the family of tetranuclear divalent sandwich complexes [M$^{II}_4$(H$_2$O)$_2$(PW$_9$O$_{34}$)$_2$]$^{10-}$ (M = Co, Cu, Zn, Mn) based on the B-type trivacant derivative of the parent Keggin structure. This structural type was first reported by Weakley, Tourné, and co-workers[14] and subsequently characterized by Finke,[15] Weakley,[16] and Gómez-García et al.[17] Although a mixed-valence Mn^{II,III} Keggin sandwich compound was reported by Pope and co-workers,[18] **1** represents

---

[†] Dedicated to Professor Achim Müller on the occasion of his 60th birthday.

[‡] Department of Chemistry, University of Rochester, Rochester, NY 14620.

[⊗] Abstract published in *Advance ACS Abstracts,* August 1, 1997.

(1) Que, L., Jr.; Ho, R. Y. N. *Chem. Rev.* **1996**, *96*, 2607−2624.

(2) Holm, R. H.; Kennepohl, P.; Solomon, E. I. *Chem. Rev.* **1996**, *96*, 2239−2314.

(3) Kurtz, J.; Donald, M. *Chem. Rev.* **1990**, *90*, 585−606.

(4) Wilkinson, B.; Zhu, M.; Priestley, N. D.; Nguyen, H.-H. T.; Morimoto, H.; Williams, P. G.; Chan, S. I.; Floss, H. G. *J. Am. Chem. Soc.* **1996**, *118*, 921−922.

(5) Representative studies of non-heme Fe complexes to model the active site in enzymes such as MMO: (a) Vincent, J. B.; Huffman, J. C.; Christou, G.; Li, Q.; Nanny, M. A.; Hendrickson, D. N.; Fong, R. H.; Fish, R. H. *J. Am. Chem. Soc.* **1988**, *110*, 6898−6900. (b) Nam, W.; Valentine, J. S. *New J. Chem.* **1989**, *13*, 677−682. (c) Leising, R. A.; Norman, R. E.; Que, L., Jr. *Inorg. Chem.* **1990**, *29*, 2553−2555. (d) Sheu, C.; Sobkowiak, A.; Jeon, S.; Sawyer, D. T. *J. Am. Chem. Soc.* **1990**, *112*, 8212−8214. (e) Leising, R. A.; Zang, Y.; Que, L., Jr. *J. Am. Chem. Soc.* **1991**, *113*, 8555−8557. (f) Fish, R. H.; Konings, M. S.; Oberhausen, K. J.; Fong, R. H.; Yu, W. M.; Christou, G.; Vincent, J. B.; Coggin, D. K.; Buchanan, R. M. *Inorg. Chem.* **1991**, *30*, 3002−3006. (g) Nam, W.; Ho, R.; Valentine, J. S. *J. Am. Chem. Soc.* **1991**, *113*, 7052−7054. (h) Stassinopoulos, A.; Schulte, G.; Papaefthymiou, G. C.; Caradonna, J. P. *J. Am. Chem. Soc.* **1991**, *113*, 8686−8697. (i) Kang, C.; Redman, C.; Cepak, V.; Sawyer, D. T. *Bioorg. Med. Chem.* **1993**, *1*, 125−140. (j) Ménage, S.; Vincent, J.-M.; Lambeaux, C.; Chottard, G.; Grand, A.; Fontecave, M. *Inorg. Chem.* **1993**, *32*, 4766−4773. (k) Kim, J.; Harrison, R. G.; Kim, C.; Que, L., Jr. *J. Am. Chem. Soc.* **1996**, *118*, 4373−4379. (l) Nguyen, C.; Guajardo, R. J.; Mascharak, P. K. *Inorg. Chem.* **1996**, *35*, 6273−6281.

(6) Representative papers on the synthetically oriented Gif systems: (a) Barton, D. H. R.; Dollar, D. *Acc. Chem. Res.* **1992**, *25*, 504−512. (b) Barton, D. H. R.; Bévière, S. D.; Chavasiri, W.; Csuhai, E.; Doller, D.; Liu, W.-G. *J. Am. Chem. Soc.* **1992**, *114*, 2147−2156. (c) Balavoine, G.; Barton, D. H. R.; Geletti, Y. V.; Hill, D. R. In *Activation of Dioxygen and Homogeneous Catalytic Oxidation*; Barton, D. H. R., Martell, A. E., Sawyer, D. T., Eds.; Plenum Press: New York, 1993; pp 225−242. (d) Singh, B.; Long, J. R.; Papaefthymiou, G. C.; Stavropoulos, P. *J. Am. Chem. Soc.* **1996**, *118*, 2147−2156 and references cited therein.

(7) Rosenzweig, A. C.; Lippard, S. J. *Acc. Chem. Res.* **1994**, *27*, 229−236.

(8) Que, L., Jr.; Dong, Y. *Acc. Chem. Res.* **1996**, *29*, 190−196.

(9) Khenkin, A. M.; Hill, C. L. *Mendeleev Commun.* **1993**, 140−141.

(10) Neumann, R.; Gara, M. *J. Am. Chem. Soc.* **1994**, *116*, 5509−5510.

(11) Neumann, R.; Gara, M. *J. Am. Chem. Soc.* **1995**, *117*, 5066−5074.

(12) Neumann, R.; Khenkin, A. M. *Inorg. Chem.* **1995**, *34*, 5753−5760.

(13) Zhang, X.; Chen, Q.; Duncan, D. C.; Campana, C.; Hill, C. L. *Inorg. Chem.* **1997**, *36*, 4208−4215.

(14) Weakley, T. J. R.; Evans, H. T., Jr.; Showell, J. S.; Tourné, G. F.; Tourné, C. M. *J. Chem. Soc., Chem. Commun.* **1973**, 139−140.

(15) Finke, R. G.; Droege, M.; Hutchinson, J. R.; Gansow, O. *J. Am. Chem. Soc.* **1981**, *103*, 1587−1589.

(16) Weakley, T. J. R.; Finke, R. G. *Inorg. Chem.* **1990**, *29*, 1235−1241.

(17) Gómez-García, C. J.; Coronado, E.; Gómez-Romero, P.; Casañ-Pastor, N. *Inorg. Chem.* **1993**, *32*, 3378−3381.
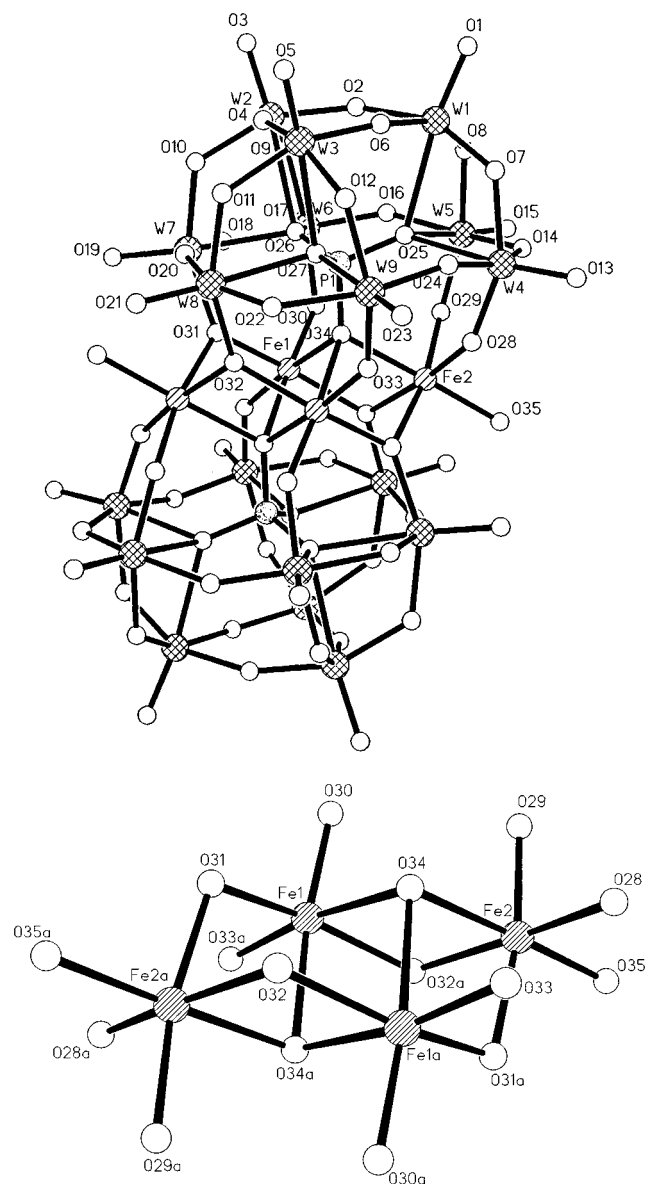
Figure 1. Top: structure of [Fe₄(H₂O)₂(PW₉O₃₄)₂]⁶⁻, **1**. Bottom: structure of the central $Fe_4(H_2O)_2O_{14}$ unit in **1**.

the only tetranuclear Keggin-derived sandwich compound containing only trivalent transition metal ions in the center. In this paper, we report the synthesis, characterization, X-ray structure, and representative H_2O_2-based alkene oxidations catalyzed by [(*n*-C₄H₉)₄N]₆[Fe^{III}₄(H₂O)₂(PW₉O₃₄)₂] (TBA-**1**).

Experimental Section

General Methods. Δ-Na₈H[PW₉O₃₄] was prepared by the literature method,[15] and its purity was checked by infrared spectroscopy. The preparation of the tetra-*n*-butylammonium (TBA) salt of the tetranuclear ferric Wells−Dawson-derived sandwich of formula [Fe^{III}₄(H₂O)₂-(P₂W₁₅O₅₆)₂]$^{12-}$ (TBA-**2**) was reported previously.[13] Acetonitrile was purchased from Burdick and Jackson. All other chemicals were the best available reagent grade compounds from Aldrich or Alfa. Infrared spectra and electronic absorption spectra were recorded on a Nicolet 510 FTIR spectrometer and a Shimadzu UV-2101 PC UV−visible spectrophotometer, respectively. Cyclic voltammograms were recorded on a standard PAR instrument with a glassy carbon disk as the working electrode (Bioanalytical Systems), a Pt wire as the auxiliary electrode, and a saturated calomel electrode in 1 M NaCl solution as the reference electrode. Average magnetic susceptibilities were measured on a

Johnson Matthey Model MSB-1 magnetic susceptibility balance as neat powders at 24 °C. EPR measurements were made at X-band using a Bruker ER 200D spectrometer equipped with a helium cryostat at 8, 50, 200, and 297 K. Mössbauer spectra were recorded on a weak-field Mössbauer spectrometer equipped with a Janis 8DT cryostat. Organic product distributions were quantified by gas chromatography (GC: Hewlett-Packard 5890 gas chromatograph equipped with a flame ionization detector and a 5% phenyl methyl silicone capillary column with nitrogen as a carrier gas) and by gas chromatography−mass spectrometry (GC/MS: Hewlett-Packard 5890 Series II GC coupled with a Hewlett-Packard 5971A mass selective detector). C, H, and N analyses were performed by Atlantic Microlab Inc., Norcross, GA. All other analyses were performed by the E&R Microanalytical Laboratory, Inc., Corona, NY.

Synthesis of [(*n*-C₄H₉)₄N]₆[Fe^{III}₄(H₂O)₂(PW₉O₃₄)₂] (TBA-1). To a solution of ferrous chloride tetrahydrate (FeCl₂·4H₂O, 0.48 g) in 25 mL of H₂O was added slowly as a solid 3.0 g of Δ-Na₈H[PW₉O₃₄] with vigorous stirring. After the solution was heated to 60 °C for ∼10 min, it was filtered hot through a medium frit. Potassium chloride (3.6 g) was added to precipitate a dark solid. The precipitate was collected and dried under water aspirator vacuum for 1 h. TBACl (2.4 g) dissolved in 300 mL of CH₂Cl₂ was added to a solution of the dark solid (∼3 g) in 100 mL of H₂O, and the two-layer mixture was shaken in a separatory funnel to afford a cloudy yellow upper layer with yellow precipitates and a clear dark brown lower layer. The bottom organic layer was collected and left in a recrystallizing dish open to the air. Over a period of 24 h, the color changed from dark brown to light brown. This solution was then concentrated to an oil using a rotary evaporator. After being washed with ca. 150 mL of H₂O, the dark oil was converted to a greenish yellow powder. The powder was collected on a medium frit and washed again with excess H₂O. After being dried under vacuum, the powder was dissolved in ca. 3−5 mL of CH₃CN, forming a dark brownish-green solution. To this solution was added ca. 150 mL of diethyl ether, resulting in a light yellow powder that was collected and dried under vacuum overnight. The yield was ca. 1.2 g (∼30%). The compound was recrystallized by dissolving 0.05 g of the crude product in 4 mL of a 5:1 v/v mixture of CH₂Cl₂ and CH₃-CN, followed by ether diffusion at −20 °C in a freezer for several days. IR (2% KBr pellet, 1300−400 cm⁻¹): 1066 (m), 1014 (w), 970 (m), 950 (m, sh), 932 (m, sh), 868 (s), 823 (s), 769 (s), 702 (s), 625 (w), 589 (w, sh), 521 (w), 496 (w, sh), 455 (w). Electronic spectral data (400−800 nm, in CH₃CN) [λ, nm (ϵ, M⁻¹ cm⁻¹)]: 485.8 (sh, 144). Anal. Calcd for C₉₆H₂₂₀Fe₄N₆O₇₀P₂W₁₈, [(*n*-C₄H₉)₄N]₆ [Fe^{III}₄(H₂O)₂-(PW₉O₃₄)₂]: C, 18.68; H, 3.59; Fe, 3.62; N, 1.36; P, 1.00; W, 53.60. Found: C, 18.73; H, 3.55; Fe, 3.35; N, 1.33; P, 0.89; W, 53.24.

X-ray Crystallographic Study of [(*n*-C₄H₉)₄N]₆[Fe^{III}₄(H₂O)₂(PW₉-O₃₄)₂]·4CH₃CN·2CH₂Cl₂·2H₂O (TBA-1). To obtain X-ray-quality crystals, the compound was recrystallized by dissolving 0.02 g of the crude product in 10 mL of a 9:1 v/v mixture of CH₂Cl₂ and CH₃CN, followed by ether diffusion at −20 °C in a freezer for ca. 1 week. A yellow rhombic crystal (0.18 × 0.12 × 0.12 mm) on a glass fiber was centered in a cold stream (−110 °C) on a standard Siemens SMART CCD Area Detector System equipped with a normal-focus molybdenum-target X-ray tube. A total of 1321 frames of data (1.3 hemispheres) were collected using a narrow-frame method with scan widths of 0.3° in ω and exposure times of 30 s/frame using a detector-to-crystal distance of 5.094 cm (maximum 2θ angle of 56.52°). Frames were integrated with the Siemens SAINT program to yield a total of 92 618 reflections, of which 21 016 were unique. The reflections were then corrected for absorption. The structure was solved by direct methods[19] in the orthorhombic space group *Pbca* (No. 61), which yielded all heavy atoms (W and Fe) and a few oxygen atoms with R_E = 0.163. The subsequent several cycles of difference Fourier synthesis gave the complete structure model with R_1 = 0.0886 ($F_o > 4\sigma(F_o)$). During final stages of full-matrix-least-squares refinement,[20] anisotropic temperature factors were employed for all non-hydrogen atoms in the anion, while isotropic temperature factors were applied to all non-hydrogen atoms in the cation, solvent, and water molecules. Hydrogen atoms

(18) Zhang, X. Y.; Jameson, G. B.; O'Connor, C. J.; Pope, M. T. *Polyhedron* **1996**, *15*, 917−922.

(19) *SHELXTL PC*; Siemens Analytical X-ray Instruments, Inc.: Madison, WI, 1990.

(20) Sheldrick, G. M. *SHELX 93: Program for structure refinement*; University of Goettingen: Goettingen, Germany, 1993.

Table 1. Crystal Data for TBA-**1**·CH₃CN·CH₂Cl₂·H₂O

empirical formula	$C_{106}H_{240}Cl_4Fe_4N_{10}Na_{110}O_{72}P_2W_{18}$
fw	6543.52
cryst color	yellow
cryst shape	rhombic
cryst system	orthorhombic
space group	*Pbca* (No. 61)
a, Å	25.330(3)
b, Å	24.9326(4)
c, Å	28.4164(3)
V, Å³	17948.3(4)
Z	4
ϱ_{calcd}, Mg m⁻³	2.422
μ, mm⁻¹	11.95
$F(000)$	12 224
temp, K	163
radiation λ, Å	0.7107
θ range, deg	1.35−28.3
abs cor	empirical
no. of total reflcns	21 016
no. of reflcns with $F_o > 4\sigma(F_o)$	14 963
no. of restraints	7
no. of params	669
$R_1 [I > 2\sigma(I)]^a$	0.0693
$wR_2{}^b$	0.149
GOF	1.091

$^a R_1 = \sum||F_o| - |F_c||/\sum|F_o|.$ $^b wR_2 = \{[\sum w(F_o{}^2 - F_c{}^2)^2]/[\sum w(F_o{}^2)^2]\}^{1/2}.$

were placed at their idealized positions as fixed contributors. Large temperature factors were observed for some of the carbon atoms of the TBA cations. No further attempts were made to model them. Crystal data, details of the intensity measurements, and refinement results are summarized in Table 1. At final convergence, $R_1 = 0.0693$ and GOF = 1.09 based on 14 963 reflections with $F_o > 4\sigma(F_o)$.

Catalytic Oxidation of Alkenes. All reactions were conducted under argon at 25 °C. Most reactions were carried out in 10-mL Schlenk tubes, each equipped with a Teflon stopcock, a serum stopper, and a magnetic stirring bar. In a typical reaction, substrate (0.9 mmol) and TBA-**1** (0.004 mmol) were dissolved in 1 mL of CH₃CN and then trimethylacetonitrile or decane was added as an internal standard. The reaction was subsequently initiated by the addition of 25 μL of 30% aqueous H₂O₂. The product distributions were evaluated immediately by GC and GC/MS.

Results and Discussion

Synthesis and Physical Properties. The procedure for the preparation of this tetranuclear ferric Keggin-derived sandwich complex is significantly different from the preparation of the corresponding literature polyanions of the divalent first-row transition metal ions, $[M^{II}_4(H_2O)_2(PW_9O_{34})_2]^{10-}$ (M = Mn, Co, Cu, Zn.[14,15,17,18] It is also different from the preparation of the tetranuclear ferric Wells−Dawson-derived sandwich complex $[Fe^{III}_4(H_2O)_2(P_2W_{15}O_{56})_2]^{12-}$.[13] Several factors are important in this synthesis: (i) use of a soluble ferrous salt as a synthetic precursor, (ii) use of the correct isomeric form of Δ-Na₈H-[PW₉O₃₄], (iii) employment of stoichiometric quantities of Fe²⁺ relative to the lacunary species, and (iv) correct oxidation conditions (O₂ oxidation in a nonaqueous aprotic solvent). A dark amorphous material precipitates from the aqueous solution after addition of potassium chloride. This is most likely the tetranuclear ferrous sandwich complex $[Fe^{II}_4(H_2O)_2(PW_9O_{34})_2]^{10-}$, as its infrared spectrum matches band for band with the infrared spectra of the well-characterized literature divalent sandwich complex $[Co^{II}_4(H_2O)_2(PW_9O_{34})_2]^{10-}$ (Figure S7, Supporting Information).[14,15] After oxidation by O₂ in a nonaqueous medium, the light yellow TBA-**1** is obtained in ca. 30% yield. In contrast, the infrared spectrum of TBA-**1**, while it has some
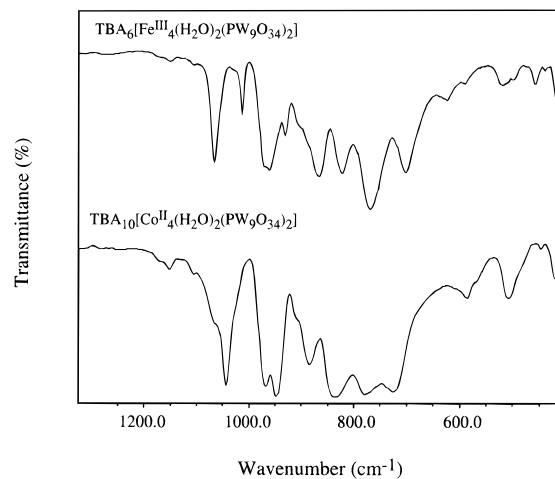
Figure 2. IR spectra of TBA-**1** (top) and a representative isostructural tetranuclear divalent metal sandwich complex, $(TBA)_{10}[Co^{II}_4(H_2O)_2(PW_9O_{34})_2]$ (bottom).
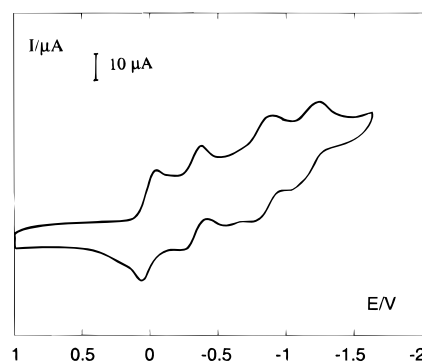
Figure 3. Cyclic voltammogram of TBA-**1** in acetonitrile vs SCE (1 M NaCl). [TBA-**1**] = 1.9 mM; supporting electrolyte 40 mM (TBA)-PF₆; scan rate 100 mV/s; 25 °C.

similarities, is distinct from those of the other divalent Keggin sandwich complexes (Figure 2).[21]

In contrast to the recently reported tetranuclear ferric Wells−Dawson-derived sandwich polyoxoanion complex of formula $[Fe^{III}_4(H_2O)_2(P_2W_{15}O_{56})_2]^{12-}$ (TBA-**2**),[13] TBA-**1** can only be prepared from a ferrous precursor. The likely reason for this difference derives from pH effects. The initial pH values of the ferrous and ferric reactant solutions are 6 and 1, respectively.

If the dark initially formed amorphous material is oxidized in aqueous solution, a slightly darker yellow solid is obtained after conversion to the TBA salt. This yellow solid has an infrared spectrum different from that of TBA-**1**. No crystalline material can be obtained when this yellow solid is subjected to the recrystallization procedure described in the Experimental Section. A series of yellow solids can be isolated from the aqueous solution initially containing Fe²⁺ and $[PW_9O_{34}]^{9-}$ as it slowly oxidizes in air, as indicated by the infrared spectra (a series of complicated and time-dependent spectra, Figure S8, Supporting Information) and catalytic behavior (significantly varying reactivity and selectivity). Repeated efforts to isolate and crystallize these labile intermediate species were unsuccessful.

The cyclic voltammogram of TBA-**1** (Figure 3) shows two cathodic peaks at −0.042 and −0.38 V (vs SCE in 1 M NaCl) and two anodic peaks at 0.062 and −0.25 V corresponding to the $Fe^{3+/2+}$ redox process. The rest potential of a solution of TBA-**1** is 0.14 V, which is more positive than the first $Fe^{3+/2+}$

(21) Zhang, X.; Sasaki, K.; Hill, C. L. *J. Am. Chem. Soc.* **1996**, *118*, 4808−4816.

Table 2. Selected Bond Lengths (Å) and Fe-to-P Distances (Å) in **1**[a]

W–O$_t$	1.707(10)	W–O$_b$	1.907(9)
W–O$_d$	2.417(8)	P1–O$_d$	1.529(9)
Fe1–O30	1.877(9)	Fe1–O31	2.003(9)
Fe1–O34	2.298(9)	Fe1–O32a	2.006(8)
Fe1–O33a	1.878(8)	Fe1–O34a	2.311(9)
Fe2–O28	1.939(9)	Fe2–O29	1.944(10)
Fe2–O34	2.169(9)	Fe2–O35	2.002(9)
Fe2–O31a	2.068(9)	Fe2–O32a	2.044(8)
P1⋯Fe1	3.382(9)	P1...Fe1a	3.401(9)
P1⋯Fe2	3.301(9)		

[a] O$_t$ = terminal oxygen; O$_b$ = doubly bridging oxygen; O$_d$ = quadruply bridging oxygen.

reduction potential. The first reduction of the polyoxyanion framework occurs at −0.87 V. The yellow TBA-**1** displays no sharp maxima for the Fe-centered d–d transition bands in the visible region because the electronic spectrum is dominated by the oxygen-to-tungsten-charge-transfer bands of the polyoxoanion framework (Figure S9, Supporting Information). No Fe^{II}-to-W^{VI} intervalence charge transfer (IVCT) transition is observed. The paramagnetic Fe$^{III}_4$ unit renders the P signal (both P atoms are equivalent by symmetry) too broad to be observable in the ^{31}P NMR. The magnetic moment for this compound is 9.8 μ_B at 24 °C, which implies some degree of antiferromagnetic coupling. The theoretical magnetic moment (spin-only) is 21.0 μ_B for a ferromagnetically coupled $S = 10$ system. TBA-**1** is EPR silent.

Even though the compound was prepared from a ferrous starting material, five lines of evidence are consistent with the Fe$^{III}_4$ oxidation state in TBA-**1**: First, bond-length-based valence sum calculations[22] from the X-ray structure yield an average oxidation state for Fe of 2.86 ± 0.07; second, the rest potential in the cyclic voltammogram indicates that the complex can be reduced, not oxidized; third, the charge balance requirements of cations and anions based on the X-ray structure and elemental analyses are most consistent with the Fe$^{III}_4$ oxidation state; fourth, the titration of TBA-**1** with standard Ce(SO$_4$)$_2$ indicates the compound cannot be oxidized by Ce^{4+}; and fifth (least definitive), O$_2$ readily oxidizes the dark Fe$^{II}_4$ sandwich complex in a nonaqueous medium, as evident by the gradual but complete disappearance of the strong IVCT band in the electronic absorption spectra. Although the ^{57}Fe Mössbauer spectra would have greatly aided the oxidation and spin state assignment of the Fe atoms in TBA-**1**, repeated efforts to obtain spectra failed due to excessive scattering by the tungsten atoms.

Crystal Structure. Unlike the well-documented structurally related tetranuclear M^{II} analogs with a generalized formula [M$_4$(H$_2$O)$_2$(PW$_9$O$_{34}$)$_2$]$^{10-}$ (M = Co^{II}, Cu^{II}, Mn^{II}),[14,16–18] **1** could be isolated as a hydrophobic salt since the oxidation by O$_2$ had to be conducted in a nonaqueous medium. The X-ray crystal structure indicates well-separated polyanions (**1**), TBA cations, and solvent molecules of crystallization (CH$_3$CN, CH$_2$Cl$_2$, and H$_2$O). The structure of **1**, shown in Figure 1, consists of two B-type trivacant Keggin[23,24] units, [PW$_9$O$_{34}$]$^{9-}$, linked by an Fe$_4$ unit in a centrosymmetric arrangement (C$_{2h}$ symmetry). Table 2 gives the selected bond lengths and distances between Fe and P atoms. A [PW$_9$O$_{34}$]$^{9-}$ moiety derives from the removal of three WO$_6$ octahedra from the parent α Keggin structure, [PW$_{12}$O$_{40}$]$^{3-}$. Removing three edge-sharing WO$_6$ octahedra (one edge-sharing W$_3$O$_{13}$ triad) results in a B-type [PW$_9$O$_{34}$]$^{9-}$,[15,25]

Table 3. Selected Maximum Bond Length and Atom Distance Differences (Å) in [M$_4$O$_{14}$(H$_2$O)$_2$(PW$_9$O$_{34}$)$_2$]$^{n-}$ (M = Cu^{II}, Co^{II}, Mn^{II}, Fe^{III}; n = 10 or 6)

complex	Δd(M–O)[a]	Δd(P⋯M)[b]	ref
M = Cu^{II}	0.650	0.175	17
M = Co^{II}	0.253	0.036	15
M = Mn^{II}	0.305	0.039	18
M = Fe^{III}	0.434	0.100	this work

[a] Maximum M–O bond length differences in all MO$_6$ octahedra of the M$_4$O$_{14}$(H$_2$O)$_2$ unit in [M$_4$O$_{14}$(H$_2$O)$_2$(PW$_9$O$_{34}$)$_2$]$^{n-}$ (M = Cu^{II}, Co^{II}, Mn^{II}, Fe^{III}; n = 10 or 6). [b] Maximum M-to-P distance differences in [M$_4$O$_{14}$(H$_2$O)$_2$(PW$_9$O$_{34}$)$_2$]$^{n-}$ (M = Cu^{II}, Co^{II}, Mn^{II}, Fe^{III}; n = 10 or 6).

while removing three corner-sharing WO$_6$ octahedra from three separate W$_3$O$_{13}$ triads results in an A-type [PW$_9$O$_{34}$].[19−,26] The A- and B-[PW$_9$O$_{34}$]$^{9-}$ moieties coordinate the central d-electron transition metal ions in the sandwich polyoxoanions in different ways, giving rise to structurally distinct complexes.[27] B-[PW$_9$O$_{34}$]$^{9-}$ provides seven oxygen donor atoms (one from the central PO$_4$ group and one each from the six W atoms) that are capable of coordinating the central tetrameric metal unit. In contrast, A-[PW$_9$O$_{34}$]$^{9-}$ provides six donor oxygen atoms (one each from the six W atoms) that generally coordinate a central trimeric metal unit. In **1**, two such B-[PW$_9$O$_{34}$]$^{9-}$ moieties are bonded to the central Fe$_4$ unit. Trivacant Keggin-derived sandwich polyoxoanions involving both A- and B-type trivacant units have been structurally characterized. Both types are known for the same transition metal in two cases, Co^{II} and Cu^{II}.[27] A few gross and local structural changes upon coordination of B-[PW$_9$O$_{34}$]$^{9-}$ moieties to the central Fe$_4$ unit merit further discussion.

The four Fe atoms in **1** form a plane and are placed around the crystallographic inversion center situated at the midpoint of the Fe1⋯Fe1a vector. Fe1 and Fe2 have different coordination environments. Fe1 is bonded to three oxygen atoms (O30, O31, and O34) on each B-[PW$_9$O$_{34}$]$^{9-}$. Fe2 is bonded to one water oxygen (O35), three oxygen atoms (O28, O29, and O34) of B-[PW$_9$O$_{34}$]$^{9-}$ on one side of the central Fe$_4$ plane, and two oxygen atoms (O31 and O32) on the other side. The PO$_4$ oxygen atom (O34) of each B-[PW$_9$O$_{34}$]$^{9-}$ links to three Fe atoms on each side of the plane, resulting in a central unit of four edge-sharing FeO$_6$ octahedra. This same Fe$^{III}_4$ unit is also present in the recently characterized analogous Wells−Dawson sandwich complex [Fe$^{III}_4$(H$_2$O)$_2$(P$_2$W$_{15}$O$_{56}$)$_2$]$^{12-}$.[13] In comparison with the [Cu$^{II}_4$O$_{14}$(H$_2$O)$_2$] unit in [Cu$_4$(H$_2$O)$_2$(PW$_9$O$_{34}$)$_2$]$^{10-}$, the Fe$^{III}_4$ unit in **1**, like the Co$^{II}_4$ and Mn$^{II}_4$ units in the analogous complexes, exhibits no Jahn−Taller distortion. The Cu−O bonds of all CuO$_6$ octahedra are elongated (the longest bond length is 2.55 Å) along an axial direction parallel to the Cu$^{II}_4$ plane, which gives rise to a maximum difference among all the Cu−O bonds of 0.650 Å (Table 3). In Fe$^{III}_4$, the maximum bond length difference among all Fe−O bonds is 0.434 Å, which is attributed to the differences in the types of bonding of Fe^{III} with O atoms. The absence of such distortion also places the Fe atoms more symmetrically

(22) O'Keeffe, M.; Navrotsky, A. *Structure and Bonding in Crystals*; Academic Press: New York, 1981.
(23) Keggin, J. F. *Nature* **1933**, *131*, 908.
(24) Brown, G. M.; Noe-Spirlet, M. R.; Busing, W. R.; Levy, H. A. *Acta Crystallogr.* **1977**, *B33*, 0000−0000.

(25) Tourné, C.; Revel, A.; Tourné, G.; Vendrell, M. *C. R. Seances Acad. Sci., Ser. C* **1973**, *277*, 643.
(26) Massart, R.; Contant, R.; Fruchart, J.-M.; Ciabrini, J.-P.; Fournier, M. *Inorg. Chem.* **1977**, *16*, 2916−2921.
(27) Co^{II} and Cu^{II} form different complexes with A- or B-α-PW$_9$O$_{34}^{9-}$. (a) A-α-Co$_3$(H$_2$O)$_3$(PW$_9$O$_{34}$)$_2^{12-}$: Knoth, W. H.; Domaille, P. J.; Farlee, R. D. *Organometallics* **1985**, *4*, 62. (b) B-α-Co$_4$-(H$_2$O)$_2$(PW$_9$O$_{34}$)$_2^{10-}$: Weakley, T. J. R.; Evans, H. T., Jr.; Showell, J. S.; Tourné, G. F.; Tourné, C. M. *J. Chem. Soc., Chem. Commun.* **1973**, 139−140. (c) A-α-Cu$_3$(NO$_3$)(PW$_9$O$_{34}$)$_2^{13-}$: Knoth, W. H.; Domaille, P. J.; Harlow, R. L. *Inorg. Chem.* **1986**, *25*, 1577. (d) B-α-Cu$_4$(H$_2$O)$_2$(PW$_9$O$_{34}$)$_2^{10-}$: Weakley, T. J. R.; Finke, R. G. *Inorg. Chem.* **1990**, *29*, 1235−1241.

Table 4. Average Trans-Directed Metal−Oxygen Bond Lengths (Å) in $[M_4O_{14}(H_2O)_2(PW_9O_{34})_2]^{n-}$ (M = Cu^{II}, Co^{II}, Mn^{II}, Fe^{III}; n = 10 or 6)[a]

$$M_{plane}\underset{A}{-}O\underset{B}{-}W_{belt}\underset{C}{-}O\underset{D}{-}W_{top}$$

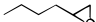| complex	A	B	C	D	ref
M = Cu^{2+}	1.933	1.784	1.995	1.870	17
M = Co^{2+}	2.024	1.842	2.027	1.870	15
M = Mn^{2+}	2.098	1.796[b]	1.957	1.889	18
M = Fe^{3+}	1.941	1.858	1.950	1.891	this work
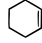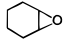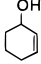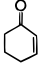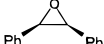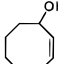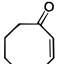
[a] M_{plane} refers to metal atoms in the $M_4O_{14}(H_2O)_2$ unit of $[M_4O_{14}(H_2O)_2(PW_9O_{34})_2]^{n-}$ (M = Cu^{II}, Co^{II}, Mn^{II}, Fe^{III}; n = 10 or 6); W_{belt} refers to the six W atoms close to the $M_4O_{14}(H_2O)_2$ unit, and W_{top} represents the three W atoms farthest away from this plane. [b] This value resulted from elimination of one erroneous data point in the calculation.

around the central P atom, as indicated by the smaller maximum P···Fe distance difference (0.100 Å). The data in Table 3 also suggest that the encapsulation of the Fe^{III}_4, Co^{II}_4, and Mn^{II}_4 units by the trivacant Keggin units gives rise to no marked perturbations of metal−oxygen bond lengths or metal−phosphorus distances.

In the Wells−Dawson-derived sandwich complexes $[M_4(H_2O)_2(P_2W_{15}O_{56})_2]^{16-}$ (M = Fe^{III}, Cu^{II}, Mn^{II}, Zn^{II}),[13,16,28,29] electronic effects give rise to significant metal−oxygen bond length alterations. Finke and Weakley[29] and Coronado et al.[28] pointed out that such bond length alterations are most pronounced in the Cu^{II}_4 complex and less so in the Zn^{II}_4 and Mn^{II}_4 analogs. In the case of Keggin-derived sandwich complexes, such phenomena are also observed. As the data in Table 4 illustrate, the Fe^{III}_4 complex has bond length alterations in the direction away from the $[M_4O_{14}(H_2O)_2]$ plane similar to those in the structurally analogous Co^{II}_4 and Mn^{II}_4 complexes and bond length alterations smaller than those in the structurally analogous Cu^{II}_4 complex.

Alkene Oxidation by H_2O_2 Catalyzed by TBA-1. TBA-**1** catalyzes the oxidation of internal alkenes by H_2O_2. Representative product distributions are given in Table 5. The catalytic effect is quite marked for some alkenes. A representative value, rate(with TBA-**1**)/rate(without TBA-**1**) is 67 for cyclohexene under the conditions given in the Experimental Section and footnote a of Table 5. TBA-**1** is inefficient as a catalyst for primary alkenes, such as 1-hexene, however. The selectivity in alkene oxidation is low. Allylic attack on aliphatic alkenes and oxidative cleavage of aromatic alkenes predominate over epoxidation. The GC traces indicate that small quantities of several other alkene-derived oxidation products, unidentifiable by GC/MS, are generated. The product distributions (allylic alcohol or ketone to epoxide ratios and overall low selectivity) are consistent with an Fe-initiated radical chain process (Fenton-type chemistry) and substrate attack by oxy radicals and/or high-valent iron−oxo intermediates. Chemoselectivity and stereoselectivity studies of Fe^{2+}/H_2O_2 in CH_3CN indicated that the intermediate hydroxyl radicals in this system are largely associated with Fe; i.e., K in eq 1 is $\gg$1.[30,31] Freely diffusing hydroxyl radicals are dominant in the classical solvent for Fenton chemistry, H_2O; i.e., K in eq 1 is $\ll$1.[32]

(28) Gómez-García, C. J.; Borrás-Almenar, J. J.; Coronado, E.; Ouahab, L. *Inorg. Chem.* **1994**, *33*, 4016−4022.
(29) Finke, R. G.; Weakley, T. J. R. *J. Chem. Crystallogr.* **1994**, *24*, 123−128.
(30) Groves, J. T.; Van Der Puy, M. *J. Am. Chem. Soc.* **1974**, *96*, 5274−5275.
(31) Groves, J. T.; Van Der Puy, M. *J. Am. Chem. Soc.* **1975**, *97*, 7118−7122.
(32) Walling, C. *Acc. Chem. Res.* **1975**, *8*, 125−131.

Table 5. Organic Products from Oxidation of Representative Alkenes with H_2O_2 Catalyzed by TBA-**1**[a]

Substrate	Products Selectivity [initial rate, mM/hr][b]		

7% [0.24]   46% [1.6]   37% [1.3]

18% [0.81]   8% [0.37]   PhCHO 65% [2.9]

45% [0.66]   0[c]   5% [0.07]

0[c]   0[c]   0[c]

[a] Reaction conditions: A solution of TBA-**1** (4 mM) and alkene substrate (0.9 M) in 1 mL of acetonitrile was degassed and stirred under Ar at 25 °C. A 30% aqueous H_2O_2 solution (25 μL) was injected to initiate the reaction. Aliquots (1.5 μL) of the reaction mixture were taken out at calibrated time intervals and analyzed by GC. [b] Selectivity = moles of indicated product/moles of all organic products derived from substrate [initial rate = slope of the indicated product concentration vs time plot at <1% conversion]. [c] Detection limit <0.2%.

Table 6. Oxidation of Cyclohexene by H_2O_2 Catalyzed by TBA-**1** and TBA-**2**[a]

	initial rate, mM/h [selectivity, %][b]				
compd	epoxide	enol	enone	yield,[c] %	stability[d]
TBA-**1**	0.21 [7]	1.6 [46]	1.3 [37]	41	stable
TBA-**2**	0.13 [11]	0.45 [40]	0.57 [48]	15	stable

[a] Reaction conditions: The same as in Table 5. [b] Initial rate = slope of the indicated product vs time plot when the conversion is less than 1% [selectivity = moles of indicated product/moles of all organic products derived from substrate]. [c] Yield = amount of cyclohexene oxidized/amount of H_2O_2 consumed, at t = 6 h. [d] Stability of TBA-**1** and TBA-**2** was checked by IR after 48 h under turnover conditions.

$$HO^{\bullet} + Fe^{3+} \rightleftharpoons Fe^{IV}{=}O + H^+ \tag{1}$$
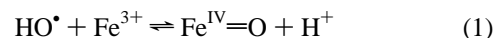
The data in Table 5 are reported as initial rates (representing several data points each) and the yields after one set reaction time (representing one data point each). This minimizes error due to subsequent oxidation of alkene-derived products under the conditions of product analysis. Product stability under turnover conditions was also assessed to further legitimate the data in Table 5. In a typical experiment, one alkene and a second alkene-derived product are stirred under catalytic conditions and the relative reactivity of the two species are quantified by GC and GC/MS analysis. For example, to assess the stability of cyclooctene-derived oxidation products, cyclohexene and cyclooctene oxide or other oxidation products compete for the substrate oxidizing species under turnover conditions. Such experiments indicate that most of the alkene-derived oxidation products are stable. For example, when the oxidation of cyclohexene is carried out with an equal concentration of cyclooctene oxide, $-\{d[cyclohexene]/dt\}$ vs $-\{d[cyclooctene\ oxide]/dt\}$ is greater than 10^3. In contrast, cyclohexene oxide is unstable under turnover conditions and is converted to diols and other products. Table 6 compares the oxidations of cyclohexene by H_2O_2 catalyzed by TBA-**1** and the ferric Wells−Dawson-derived sandwich complex (TBA-**2**). The table shows both complexes are reactive in catalyzing the oxidation of alkenes by H_2O_2 but with low selectivity for epoxide. From

the product distributions, the oxidation reactions likely operate via a similar reaction mechanism.

Unlike most previously documented transition-metal-substituted polyoxometalates (TMSPs), both TBA-**1** and TBA-**2** are relatively stable at high H_2O_2 concentration (ca. 0.25 M for the catalytic oxidation reactions). There is no significant change in the IR spectra after 48 h of incubation with ca. 0.25 M aqueous H_2O_2. Furthermore no new species are detected by ^{31}P NMR. The rates of H_2O_2 disproportionation catalyzed by both TBA-**1** and TBA-**2** were determined by iodometric titration. These rates are relatively slow compared to those for other TMSPs and are similar for TBA-**1** and TBA-**2**. Titration of H_2O_2 after 6 h of alkene oxidation indicates that the product yields based on the amount of H_2O_2 consumed are significantly higher for TBA-**1** than for TBA-**2**. This reflects the ratio of the two dominant H_2O_2-consuming processes, alkene oxidation and H_2O_2 disproportionation. Although the rates of H_2O_2 disproportionation are comparable for TBA-**1** and TBA-**2**, the rate of oxidation is greater for TBA-**1** than for TBA-**2**.

Supporting Information Available: Tables giving the structure determination summary, atomic coordinates ($\times 10^4$) and equivalent isotropic displacement coefficients ($\text{Å}^2 \times 10^3$), bond lengths (Å) and bond angles (deg), anisotropic displacement parameters ($\text{Å}^2 \times 10^3$), and hydrogen coordinates and isotropic displacement parameters and figures showing IR spectra of the dark precipitate from aqueous solution and of $K_{10}[Co_4(H_2O)_2(PW_9O_{34})_2]$, IR spectra of the TBA salts of the dark precipitate after different exposure times to air in the aqueous solution, and an electronic absorption spectrum of TBA-**1** (16 pages). Ordering information is given on any current masthead page.

IC970391R